*Supplement of*

**Machine Learning Assisted Chemical Characterization and Optical Properties of Atmospheric Brown Carbon in Nanjing, China**

Yu Huang[1], Xingru Li[2], Dan Dan Huang[3], Ruoyuan Lei[1], Binhuang Zhou[1], Yunjiang Zhang[1], Xinlei Ge[1, 4*]

[1] Jiangsu Key Laboratory of Atmospheric Environment Monitoring and Pollution Control, Collaborative Innovation Center of Atmospheric Environment and Equipment Technology, School of Environmental Science and Engineering, Nanjing University of Information Science and Technology, Nanjing 210044, China

[2] Analytical Instrumentation Center, Department of Chemistry, Capital Normal University, Beijing, 100048, China

[3] Shanghai Academy of Environmental Sciences, Shanghai 200233, China

[4] School of Environment and Energy Engineering, Anhui Jianzhu University, Hefei 230601, China

*Corresponding author: Xinlei Ge (Email: caxinra@163.com)

**Text S1**

A portion of each quartz filter (10*3.14 cm$^2$) was cut off for analysis. The piece was cut into small pieces and placed into a 30 ml brown vial. 5 mL methanol (Optima LC/MS grade, Fisher Chemical, USA) was added to the brown vial and sonicated for 30 minutes at ambient temperature, and the procedure was repeated three times. The solution was then filtrated through a 0.22 μm PTFE filter (Fisher Chemical, USA), followed by the blow-drying with nitrogen gas. The blow-dried solid residue was re-dissolved in 300 μL of methanol and transferred to a 1.5 ml brown injection vial for storage. A 30 μL aliquot from each sample was mixed together as a QC (quality check) sample.

**Text S2**

The analysis was performed by using an Acquity H Class Ultra Performance Liquid Chromatography system coupled to a Xevo G2-Xs Quadrupole time-of-flight mass spectrometer (UPLC-QTOF-MS, Agilent Technologies Inc. Santa Clara, CA, USA). A C18 column (100 mm × 2.1 mm × 1.6 μm) (Luna Omega, Phenomenex) was used for the chromatographic separation, and temperature of the column was maintained at 40 °C. The sample volume was 1.5 μL for the positive ion (ESI$^+$) mode and 3 μL for the negative ion (ESI$^-$) mode. The mobile phase was consisted of solvent A (ultrapure water containing 0.1% v/v formic acid and 5 mM ammonium acetate) and solvent B (acetonitrile containing 0.1% v/v formic acid), and the gradients of eluent were programmed as follows: 2 % B at 0 ~ 1.5 min; linearly from 2 % B to 20 % B at 1.5 ~ 11 min; linearly from 20 % B to 60 % B at 11 ~ 18 min; linearly from 60 % B to 98 % B at 18 ~ 20 min; maintain at 98 % B at 20 ~ 22min, then decrease to 2 % B at 22 ~ 25 min.

The instrument used the electrospray ionization (ESI) technique. A data independent acquisition (DIA) resolution mode was operated with a *m/z* ratio of 50-1200, a scanning interval of 0.1 s, capillary voltages of 0.7 KV for ESI$^+$ and 2.35 KV for ESI$^-$, a cone bore voltage of 30 V, an ion source temperature of 120 °C, a cone bore

48  gas of 50 L min$^{-1}$, a desolvation gas of 1000 L min$^{-1}$, and collision energies of 10 ~ 50

49  eV. The positive or negative ion modes were calibrated with leucine enkephalin and

50  sodium formate polymers, respectively, and data were acquired by using Masslynx 4.1.

51

52  **Text S3**

53  The raw UPLC-QTOF-MS data were processed using the Mass Spectrometry-

54  Data Independent Analysis (MS-DIAL, version 4.92) software, involving peak

55  extraction, peak alignment, and deconvolution with a detection probability of 70 %.

56  The summed ions included [M-H]$^-$ (ESI$^-$) and [M+H]$^+$, [M+NH$_4$]$^+$, [M+Na]$^+$ (ESI$^+$).

57  Missing data were replaced by 1/10 of the minimum value (default value: 100).

58  Chromatographic intensities were normalized using the systematic error removal using

59  random forest (a machine learning algorithm) (SERRF) software, which is based on the

60  machine learning (ML) random forest (RF) algorithm. Additionally, corrections were

61  applied for potential intensity drift.

62  By using MS-DIAL, all deconvoluted MS/MS spectra were exported as

63  individual .mat files. Subsequently, all MS/MS spectra were examined and imported

64  into SIRIUS (version 5.6.2) for the identification of molecular formulas of each *m/z*. In

65  order to obtain a more refined list of molecular formulas, specific constraints below

66  were applied, and those did not comply with these rules were excluded.

67  (1) Atomic numbers: 1~50 12C, 1 ~ 100 1H, 0 ~ 40 16O, 0 ~ 5 14N, 0 ~ 2 32S;

68  (2) Elemental ratios: In ESI$^-$ mode, 0.3 ~ 3.0 H/C, 0 ~ 3 O/C, 0 ~ 0.5 N/C, 0 ~ 2.0

69  S/C; in ESI$^+$ mode, 0.3 ~ 3.0 H/C, 0 ~ 1.2 O/C, 0 ~ 1.0 N/C, 0 ~ 0.8 S/C.

70  (3) Equivalent double bond (DBE) numbers: 0 ~ 25.

71  The double-bond equivalent (DBE) value of a molecule is used to indicate the

72  level of unsaturation, which can be calculated by using the following Eq. (S1):

73
$$DBE = \frac{2 \times C - H + N + 2}{2} \qquad (S1)$$

74  Here, C, H, N are the number of carbon, hydrogen and nitrogen in the formula of

75  the molecule. Furthermore, the aromaticity equivalent (Xc) has been used to aid the

76  identification of aromatic and condensed aromatic compounds, as described in Yassine

77 et al. (2014). Compared to the aromaticity index (AI), the advantage of Xc lies in its

78 ability to accurately classify (poly)aromatic compounds with significant alkylations.

79 The Xc value can be calculated with Eq. (S2):

80
$$X_C = \frac{3 \times \left(DBE - (p \times O + q \times S)\right) - 2}{DBE - (p \times O + q \times S)} \tag{S2}$$

81 Where $p$ and $q$ are the fractions of oxygen and sulfur atoms involved in the π-

82 bond structure of the molecule, respectively. In this study, $p = q = 0.5$ was used for the

83 compounds detected in ESI⁻, and $p = q = 1$ was selected for ESI⁺ (Kourtchev et al., 2016;

84 Tong et al., 2016) because ESI⁻ is more sensitive to compounds containing carboxylic

85 groups, and compounds with a large diversity of functional groups can possibly be

86 detected in ESI⁺. Compounds with Xc < 2.5 were considered to be non-aromatics, with

87 Xc ≥ 2.5 indicating aromatics and Xc ≥ 2.71 being considered as condensed aromatics

88 (Yassine et al., 2014).

89 The O/C, H/C and DBE of a sample was calculated over all identified molecules

90 based on their relative abundances, as follows:

91
$$O/C = \sum \left(Iin * O/C_i\right) / \sum Iin_i \tag{S3}$$

92
$$H/C = \sum \left(Iin * H/C_i\right) / \sum Iin_i \tag{S4}$$

93
$$DBE = \sum \left(Iin * DBE_i\right) / \sum Iin_i \tag{S5}$$

94 Where Ini represents the relative abundance of molecule $i$, O/C$_i$, H/C$_i$ and DBE$_i$,

95 represent the O/C, H/C and DBE of the molecule $i$, respectively.

96 Table S1. Numbers of molecules, number fractions of different types of identified
97 compounds to the total, and their average O/C, H/C and DBE values.

| | Ion mode | Molecular types | Number of molecules | Number fractions | O/C | H/C | DBE |
|---|---|---|---|---|---|---|---|
| Summer Season (SS) Daytime | ESI⁻ | Total | 466 | 100.00% | 0.24 | 1.65 | 5.25 |
| | | CH | 2 | 0.43% | 0.00 | 1.74 | 5.99 |
| | | CHO | 207 | 44.42% | 0.28 | 1.46 | 6.61 |
| | | CHN | 4 | 0.86% | 0.00 | 1.54 | 4.75 |
| | | CHS | 2 | 0.43% | 0.00 | 0.98 | 7.06 |
| | | CHON | 152 | 32.62% | 0.28 | 1.82 | 4.33 |
| | | CHOS | 22 | 4.72% | 0.22 | 1.78 | 2.89 |
| | | CHNS | 2 | 0.43% | 0.00 | 2.01 | 1.81 |
| | | CHONS | 75 | 16.09% | 0.20 | 1.70 | 5.99 |
| | ESI⁺ | Total | 644 | 100.00% | 0.17 | 1.80 | 4.55 |
| | | CH | 5 | 0.78% | 0.00 | 1.48 | 3.91 |
| | | CHO | 186 | 28.88% | 0.33 | 1.55 | 5.82 |
| | | CHN | 43 | 6.68% | 0.00 | 1.84 | 2.81 |
| | | CHS | 2 | 0.31% | 0.00 | 1.55 | 3.91 |
| | | CHON | 325 | 50.47% | 0.12 | 1.88 | 4.11 |
| | | CHOS | 3 | 0.47% | 0.21 | 1.24 | 5.40 |
| | | CHNS | 3 | 0.47% | 0.00 | 1.26 | 5.60 |
| | | CHONS | 77 | 11.96% | 0.31 | 1.73 | 7.23 |
| | ESI⁻ | Total | 518 | 100.00% | 0.26 | 1.64 | 5.41 |
| | | CH | 2 | 0.39% | 0.00 | 1.80 | 5.17 |
| | | CHO | 197 | 38.03% | 0.24 | 1.40 | 6.97 |
| | | CHN | 2 | 0.39% | 0.00 | 2.00 | 1.56 |
| | | CHS | 3 | 0.58% | 0.00 | 0.87 | 7.07 |
| | | CHON | 180 | 34.75% | 0.30 | 1.82 | 4.11 |

| | | | | | | | |
|---|---|---|---|---|---|---|---|
| | | CHOS | 25 | 4.83% | 0.20 | 1.71 | 3.21 |
| | | CHNS | 2 | 0.39% | 0.00 | 2.00 | 2.00 |
| Summer Season (SS) | | CHONS | 107 | 20.66% | 0.28 | 1.75 | 6.09 |
| Nighttime | | Total | 735 | 100.00% | 0.17 | 1.78 | 4.54 |
| | | CH | 9 | 1.22% | 0.00 | 1.73 | 2.84 |
| | | CHO | 225 | 30.61% | 0.30 | 1.55 | 5.25 |
| | | CHN | 63 | 8.57% | 0.00 | 1.82 | 2.81 |
| | ESI$^+$ | CHS | 2 | 0.27% | 0.00 | 2.04 | 0.71 |
| | | CHON | 345 | 46.94% | 0.12 | 1.87 | 4.13 |
| | | CHOS | 7 | 0.95% | 0.16 | 1.15 | 7.24 |
| | | CHNS | 9 | 1.22% | 0.00 | 1.66 | 3.39 |
| | | CHONS | 75 | 10.20% | 0.47 | 1.63 | 7.64 |
| | | Total | 729 | 100.00% | 0.29 | 1.55 | 4.92 |
| | | CH | 2 | 0.27% | 0.00 | 1.92 | 1.60 |
| | | CHO | 284 | 38.96% | 0.26 | 1.50 | 6.43 |
| | | CHN | 3 | 0.41% | 0.00 | 1.35 | 7.51 |
| | ESI$^-$ | CHS | 0 | 0.00% | 0.00 | 0.00 | 0.00 |
| | | CHON | 241 | 33.06% | 0.34 | 1.39 | 4.99 |
| | | CHOS | 34 | 4.66% | 0.20 | 1.81 | 2.53 |
| | | CHNS | 2 | 0.27% | 0.01 | 1.94 | 2.30 |
| Cold Season (CS) | | CHONS | 163 | 22.36% | 0.32 | 1.86 | 3.69 |
| Daytime | | Total | 894 | 100.00% | 0.20 | 1.80 | 4.23 |
| | | CH | 14 | 1.57% | 0.00 | 1.86 | 2.03 |
| | | CHO | 217 | 24.27% | 0.27 | 1.68 | 4.75 |
| | | CHN | 63 | 7.05% | 0.00 | 1.83 | 2.94 |
| | ESI$^+$ | CHS | 3 | 0.34% | 0.00 | 2.13 | 0.00 |
| | | CHON | 484 | 54.14% | 0.13 | 1.89 | 3.31 |
| | | CHOS | 4 | 0.45% | 0.13 | 0.94 | 9.61 |
| | | CHNS | 5 | 0.56% | 0.00 | 2.24 | 1.53 |

| | | | | | | | |
|---|---|---|---|---|---|---|---|
| | | CHONS | 104 | 11.63% | 0.47 | 1.64 | 7.91 |
| | | Total | 865 | 100.00% | 0.32 | 1.47 | 5.46 |
| | | CH | 3 | 0.35% | 0.00 | 1.91 | 2.03 |
| | | CHO | 313 | 36.18% | 0.26 | 1.49 | 6.26 |
| | | CHN | 3 | 0.35% | 0.00 | 1.03 | 9.92 |
| | ESI⁻ | CHS | 0 | 0.00% | 0.00 | 0.00 | 0.00 |
| | | CHON | 329 | 38.03% | 0.38 | 1.37 | 5.28 |
| | | CHOS | 34 | 3.93% | 0.25 | 1.71 | 3.20 |
| | | CHNS | 0 | 0.00% | 0.00 | 0.00 | 0.00 |
| Cold Season (CS) | | CHONS | 183 | 21.16% | 0.28 | 1.72 | 5.20 |
| Nighttime | | Total | 1065 | 100.00% | 0.17 | 1.76 | 4.72 |
| | | CH | 13 | 1.22% | 0.00 | 1.79 | 2.52 |
| | | CHO | 245 | 23.00% | 0.26 | 1.56 | 5.72 |
| | | CHN | 86 | 8.08% | 0.00 | 1.72 | 3.56 |
| | ESI⁺ | CHS | 3 | 0.28% | 0.00 | 2.10 | 0.35 |
| | | CHON | 587 | 55.12% | 0.14 | 1.83 | 4.37 |
| | | CHOS | 6 | 0.56% | 0.14 | 1.09 | 8.14 |
| | | CHNS | 3 | 0.28% | 0.00 | 2.44 | 0.44 |
| | | CHONS | 122 | 11.46% | 0.44 | 1.66 | 7.10 |
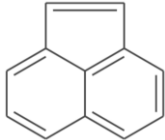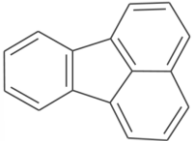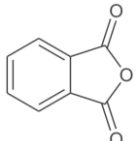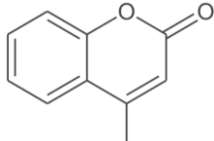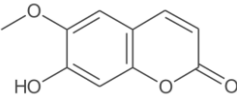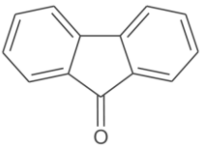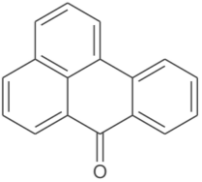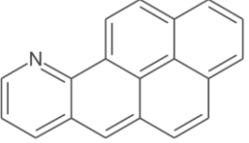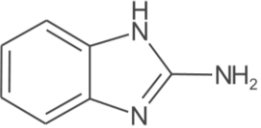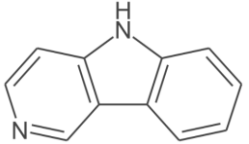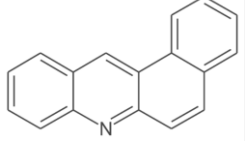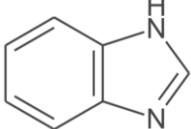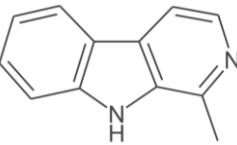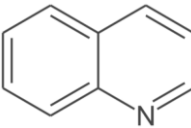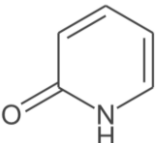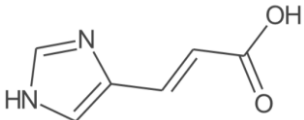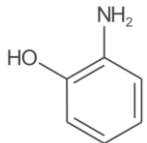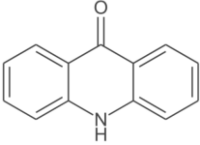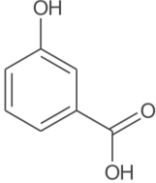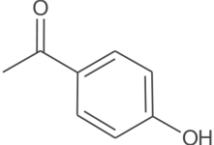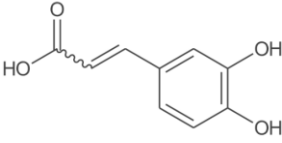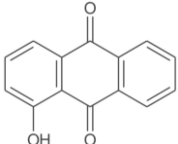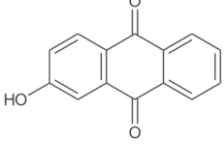
98
99
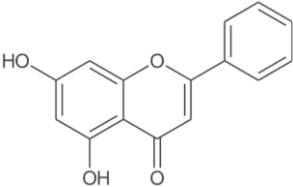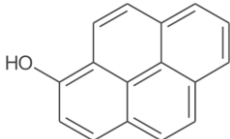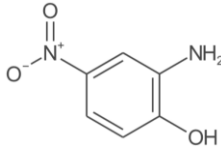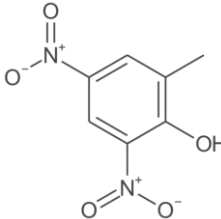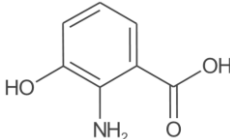
Table S2. Identified key light-absorbing compounds (BrC) assisted by the machine learning (a corresponding reference provides that this compound has been reported as a BrC species)
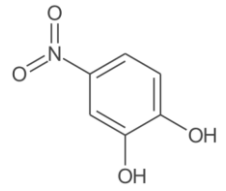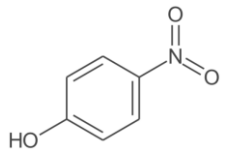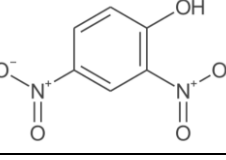
| Retention time | m/z | Proposed name | Proposed molecular formula | Proposed structure | Proposed molecular type | References |
|---|---|---|---|---|---|---|
| ESI⁺ | | | | | | |
| 14.967 | 152.0624 | Acenapthylene | C12H8 |  | PAH | (Aurell et al., 2015) |
| 18.431 | 202.0788 | Fluoranthene | C16H10 |  | PAH | (Kuang et al., 2021) |
| 19.812 | 149.0238 | Phthalic anhydride | C8H4O3 |  | O-Heterocyclic | (Chen et al., 2022) |
| 20.67 | 161.0604 | 4-Methylcoumarin | C10H8O2 |  | O-Heterocyclic | This work |
| 8.908 | 193.05 | Scopoletin | C10H8O4 |  | O-Heterocyclic | (Zhang, 2018) |

| | | | | | | |
|---|---|---|---|---|---|---|
| 14.987 | 181.0648 | 9-Fluorenone | C13H8O |  | PAOH | (Kuang et al., 2023) |
| 17.656 | 231.0816 | Benzanthrone | C17H10O |  | PAOH | (Kuang et al., 2023) |
| 18.533 | 254.0966 | 10-Azabenzo[a]pyrene | C19H11N |  | N-PAH | This work |
| 0.756 | 134.0712 | 2-Aminobenzimidazole | C7H7N3 |  | N-Heterocyclic | This work |
| 7.49 | 169.0761 | 5-Carboline | C11H8N2 |  | N-Heterocyclic | (Ma and Hays, 2008) |
| 16.29 | 230.0968 | Benz[c]acridine | C17H11N |  | N-PAH | This work |

| | | | | | | |
|---|---|---|---|---|---|---|
| 1.807 | 119.0604 | Benzimidazole | C7H6N2 |  | N-Heterocyclic | This work |
| 9.223 | 183.0922 | Harmane | C12H10N2 |  | N-Heterocyclic | (Ma and Hays, 2008) |
| 1.102 | 130.0651 | Quinoline | C9H7N |  | Quinoline | This work |
| 1.301 | 96.0443 | 2-Hydroxypyridine | C5H5NO |  | Pyridones | This work |
| 0.863 | 121.0395 | Urocanate | C6H6N2O2 |  | Carboxylic Acids | This work |
| 1.14 | 110.06 | 2-Aminophenol | C6H7NO |  | Aminophenol | (Al-Abadleh et al., 2022) |

| | | | | | | |
|---|---|---|---|---|---|---|
| 13.021 | 196.076 | Acridone | C13H9NO |  | Acridone | (Negron-Encarnacion and Arce, 2007) |
| ESI⁻ | | | | | | |
| 4.113 | 137.0212 | 3-hydroxybenzoic acid | C7H6O3 |  | Carboxylic acid | This work |
| 7.566 | 135.0424 | 4-Hydroxyacetophenone | C8H8O2 |  | Phenol | This work |
| 7.567 | 179.0325 | trans-Caffeic acid | C9H8O4 |  | Carboxylic acid | (Le Person et al., 2013) |
| 15.434 | 223.0372 | 1-Hydroxyanthraquinone | C14H8O3 |  | Quinone | (Kuang et al., 2023) |
| 13.817 | 223.0372 | 2-Hydroxyanthraquinone | C14H8O3 |  | Quinone | This work |

| | | | | | | |
|---|---|---|---|---|---|---|
| 16.344 | 253.048 | Chrysin | C15H10O4 |  | Benzopyrans | This work |
| 17.937 | 217.0632 | 1-Hydroxypyrene | C16H10O |  | Hydroxyl-PAHs | (Huang et al., 2022) |
| 6.45 | 153.0276 | 2-Amino-4-nitrophenol | C6H6N2O3 |  | Nitrophenol | This work |
| 14.806 | 197.0176 | 2-Methyl-4,6-dinitrophenol | C7H6N2O5 |  | Nitrophenol | (Li et al., 2020) |
| 12.293 | 152.0322 | 3-Hydroxyanthranilic acid | C7H7NO3 |  | Aminophenol | This work |

| | | | | | | |
|---|---|---|---|---|---|---|
| 6.556 | 154.0118 | 4-Nitrocatechol | C6H5NO4 |  | Nitrophenol | (Li et al., 2020) |
| 8.781 | 138.0173 | 4-Nitrophenol | C6H5NO3 |  | Nitrophenol | (Li et al., 2020) |
| 10.487 | 183.0017 | 2,4-Dinitrophenol | C6H4N2O5 |  | Nitrophenol | (Li et al., 2020) |
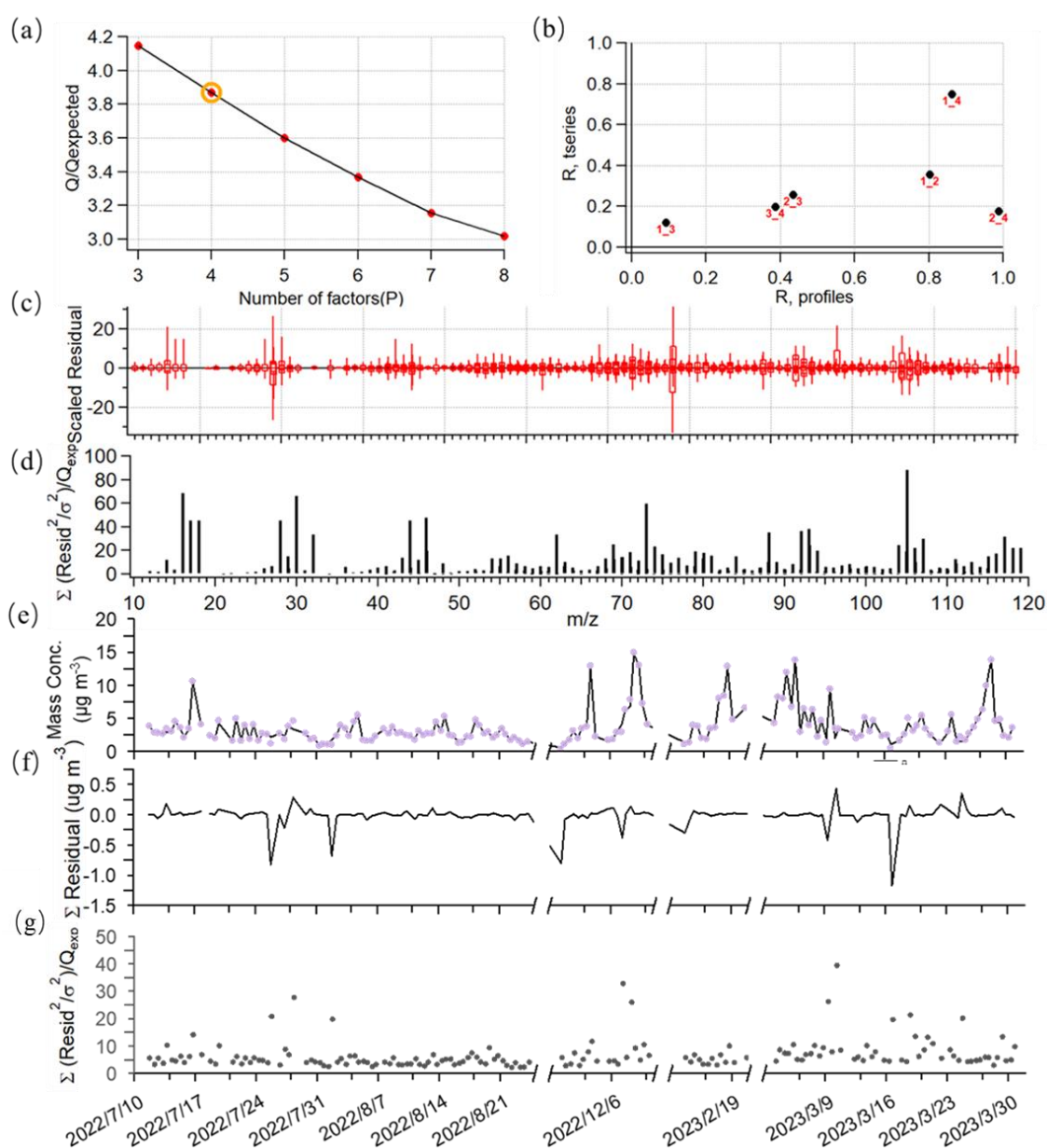
Figure S1. Summary of critical diagnostic plots of the PMF results for the 4-factor solution of WSOA: (a) $Q/Qexp$ as a function of the number of factors (P from 3 to 8). For the best solution (4-factor); (b) cross-correlations of the time series and spectral profiles among the four factors; (c) the box and whiskers plot showing the distributions of scaled residuals for each $m/z$; (d) the $Q/Qexp$ values for each $m/z$; (e) time series of the measured and the reconstructed WSOA mass loadings; (f) variations of the residuals of the fit; (g) the $Q/Qexp$ values for each sample.
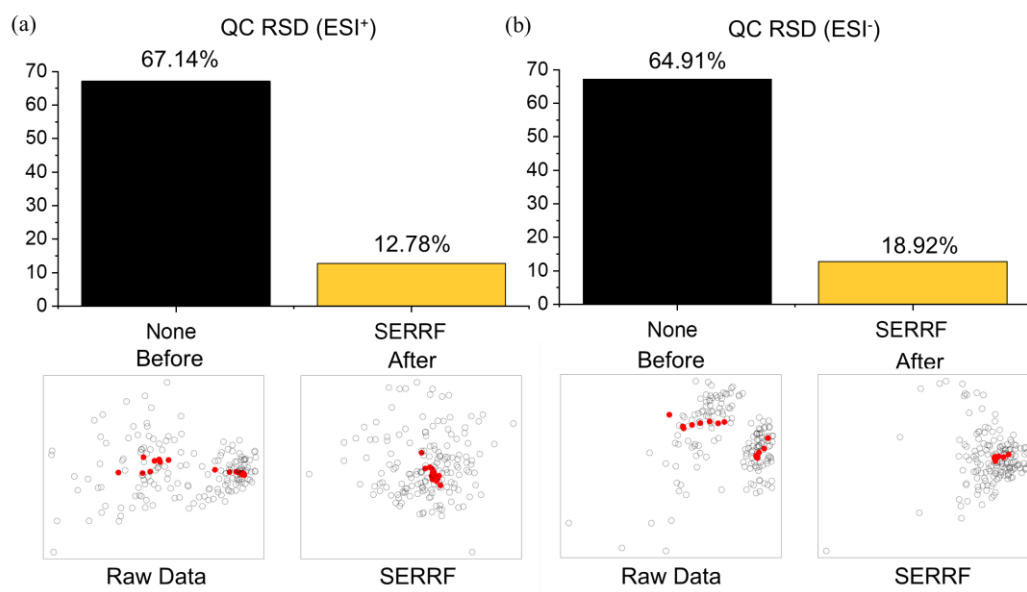
Figure S2. Relative standard deviations before and after the SERRF normalization (The gray and red markers represent real samples and QC samples, respectively). (a) ESI⁺ mode, (b) ESI⁻ mode.
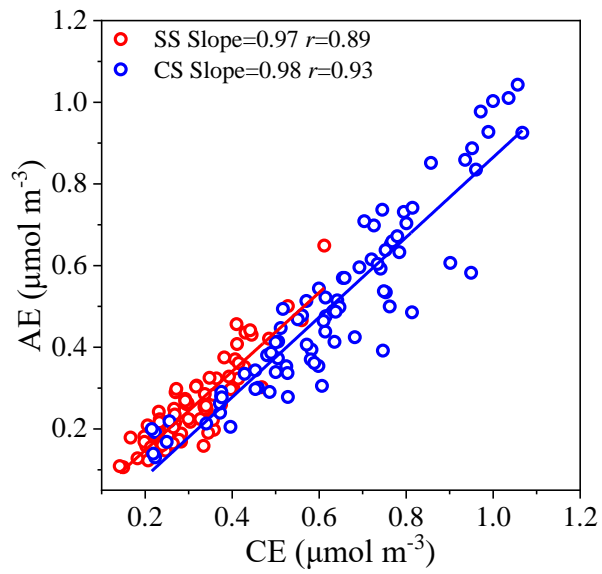
Figure S3. Scatter plot of the molar concentrations of cations versus anions (SS: Summer season; CS: Cold season).
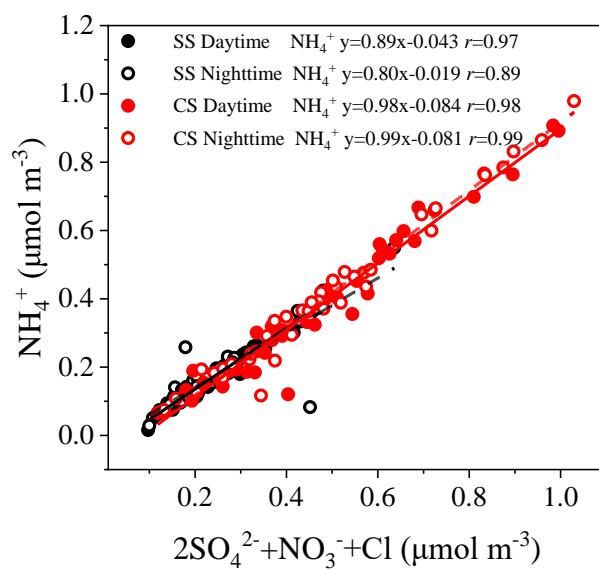
Figure S4. Scatter plot of the molar concentrations of ammonium versus sum of sulfate, nitrate and chloride (SS: Summer season; CS: Cold season).
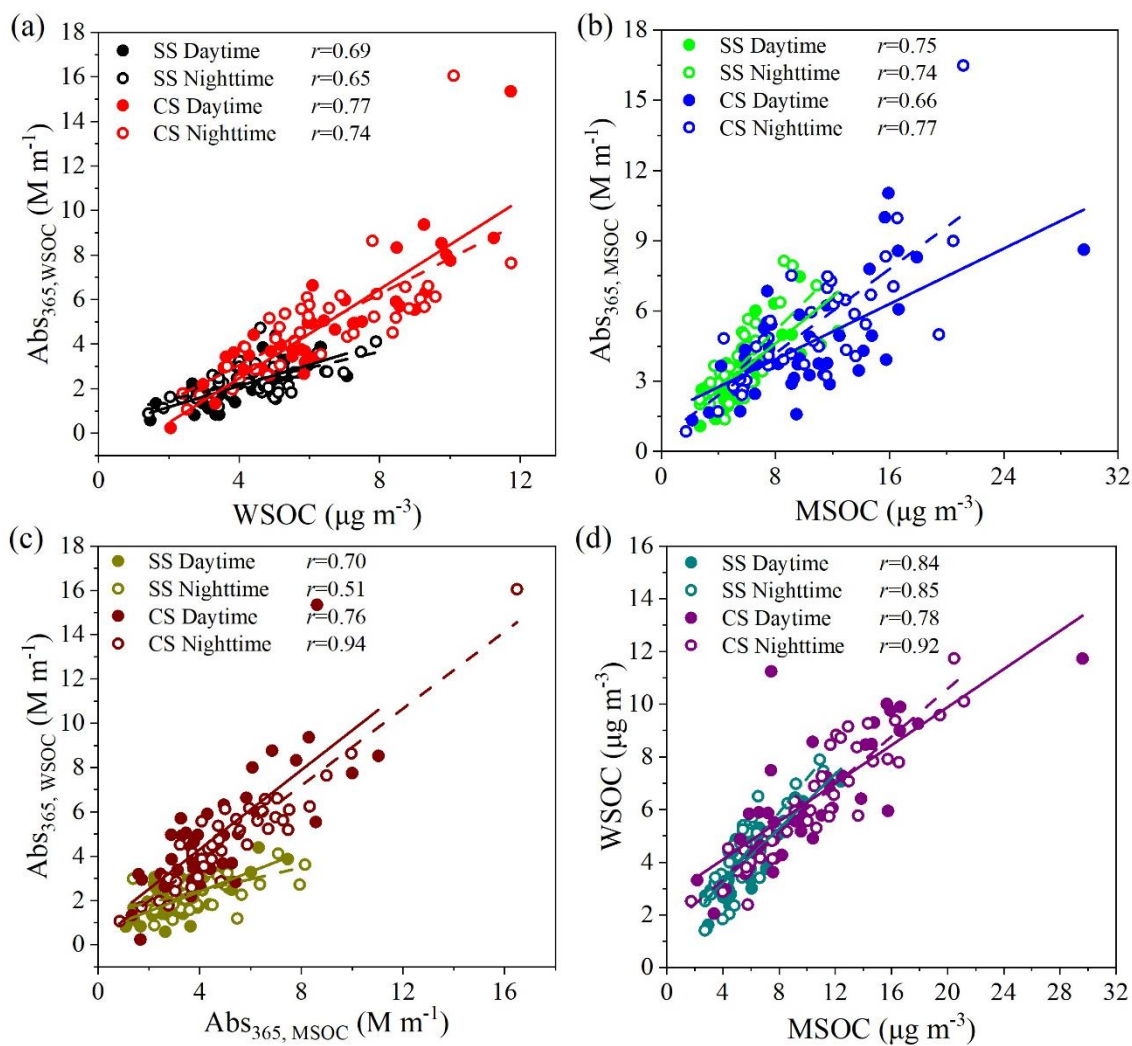
Figure S5. Scatter plots of: (a) light absorption at 365 nm of WSOC (Abs$_{365, WSOC}$) versus WSOC concentrations; (b) light absorption at 365 nm of MSOC (Abs$_{365, MSOC}$) versus MSOC concentrations; (c) WSOC versus MSOC, and (d) Abs$_{365, WSOC}$ versus Abs$_{365, MSOC}$.
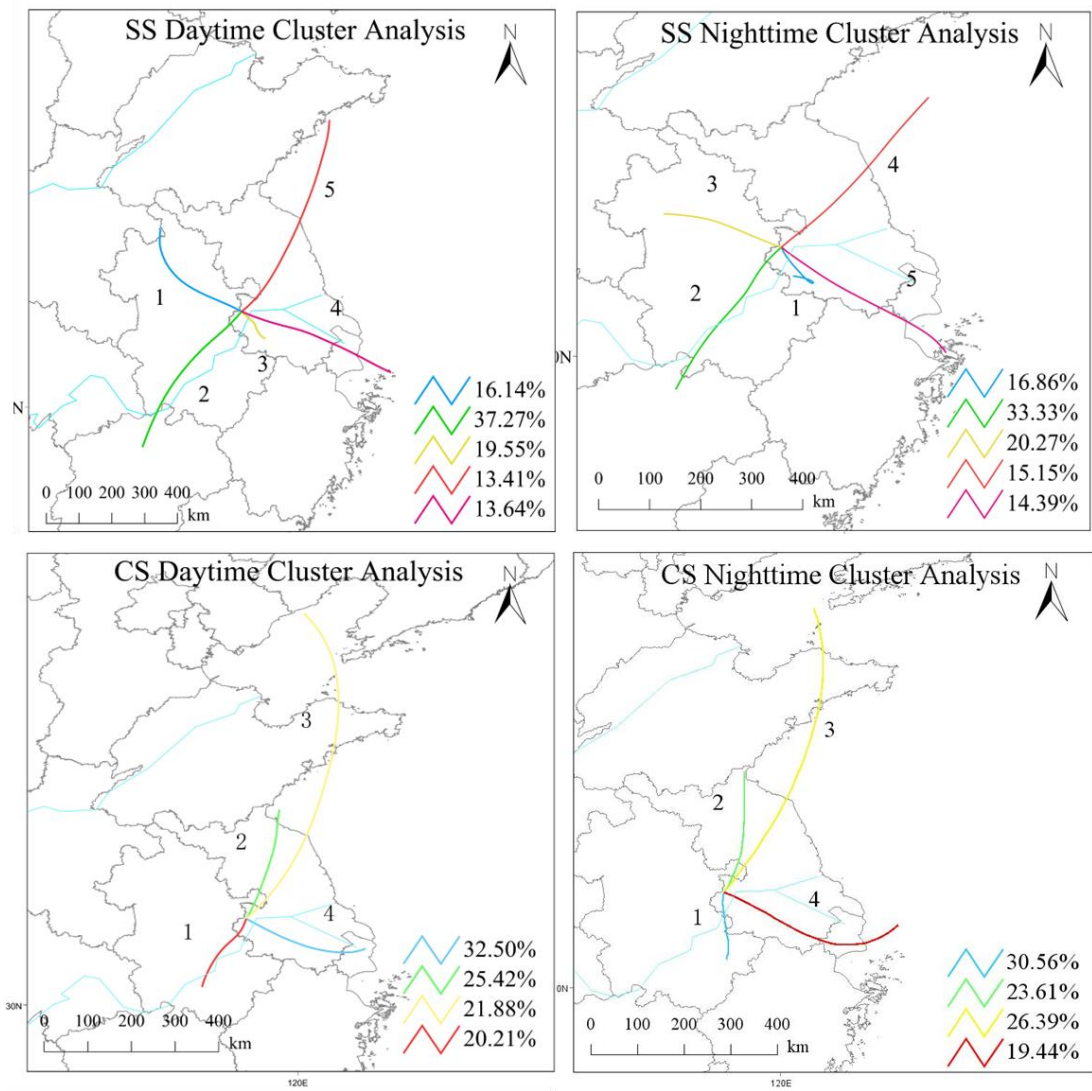
Figure S6. Clustered backward trajectories of different sampling periods.
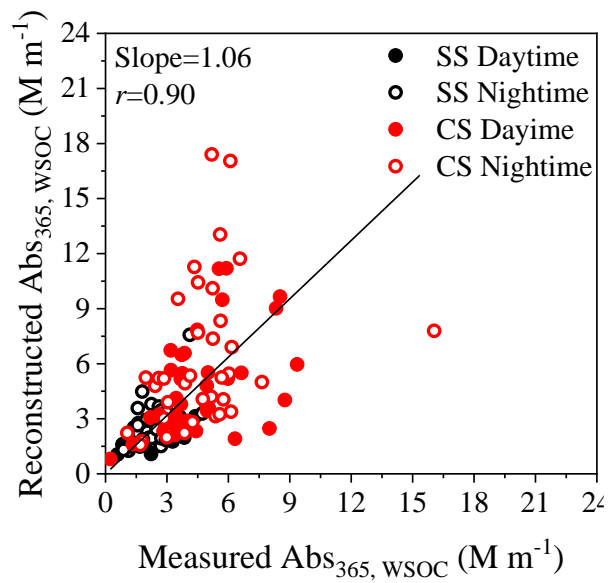
Figure S7. Scatter plot of the reconstructed Abs$_{365}$ from the multilinear regression versus measured Abs$_{365}$.
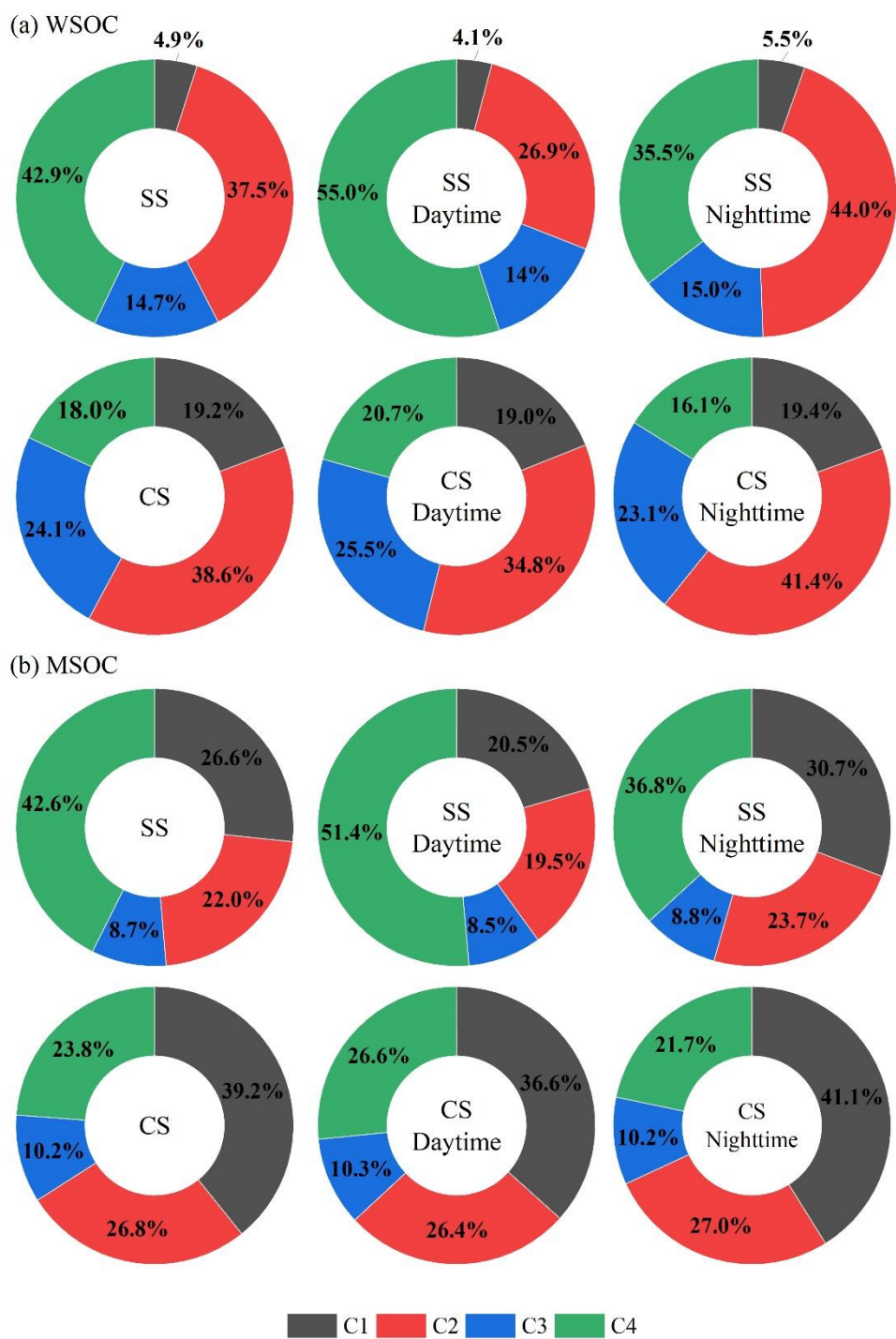
Figure S8. Average contributions of the PARAFAC-derived fluorescent components of (a) WSOC and (b) MSOC during different periods.
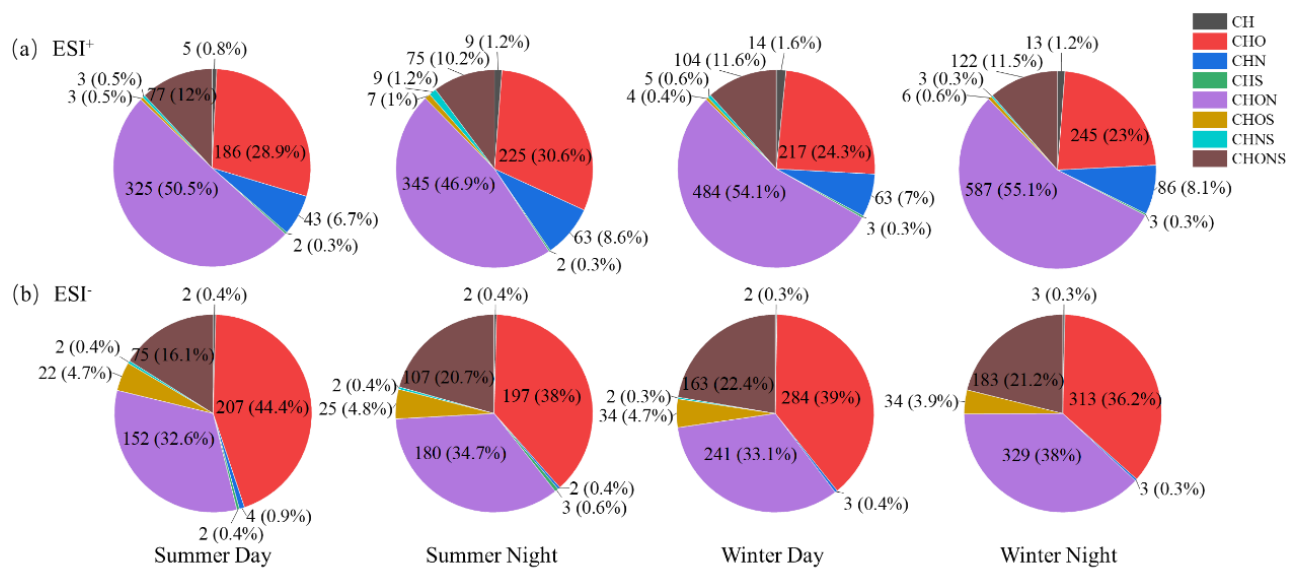
Figure S9. Numbers and number fractions of different types of compounds identified during different periods. (a) ESI$^+$ mode, (b) ESI$^-$ mode.
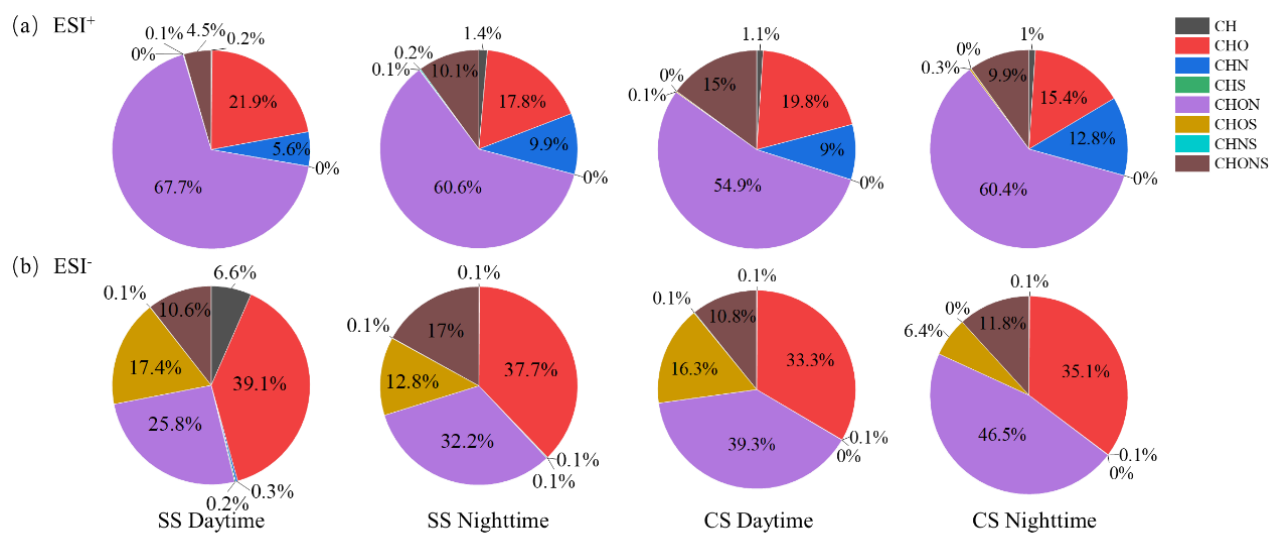
Figure S10. Contributions of the signal relative abundance of different types of compounds identified during different periods. (a) ESI⁺ mode, and (b) ESI⁻ mode.
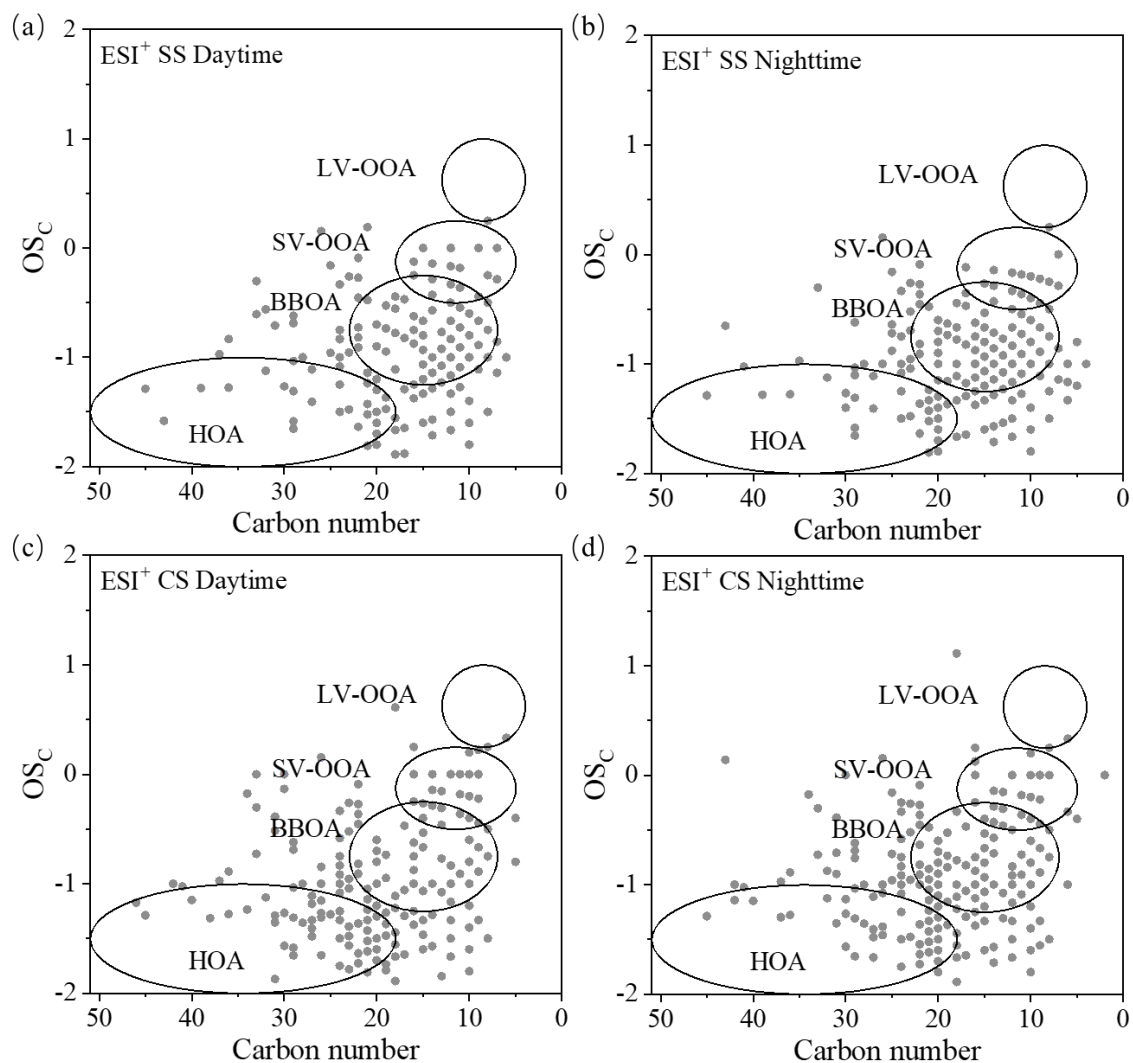
Figure S11. Scatter plots of the carbon oxidation state (OSc) versus carbon number for all CHO compounds in ESI$^+$ mode during diffeent periods. (a) SS daytime, (b) SS nighttime, (c) CS daytime, and (d) CS nighttime. The circled areas represent those from fossil fuel combustion hydrocarbon-like OA (HOA), biomass burning OA (BBOA), semi-volatile oxygenated OA (SV-OOA) and low-volatility oxygenated OA (LV-OOA) (Kroll et al., 2011).
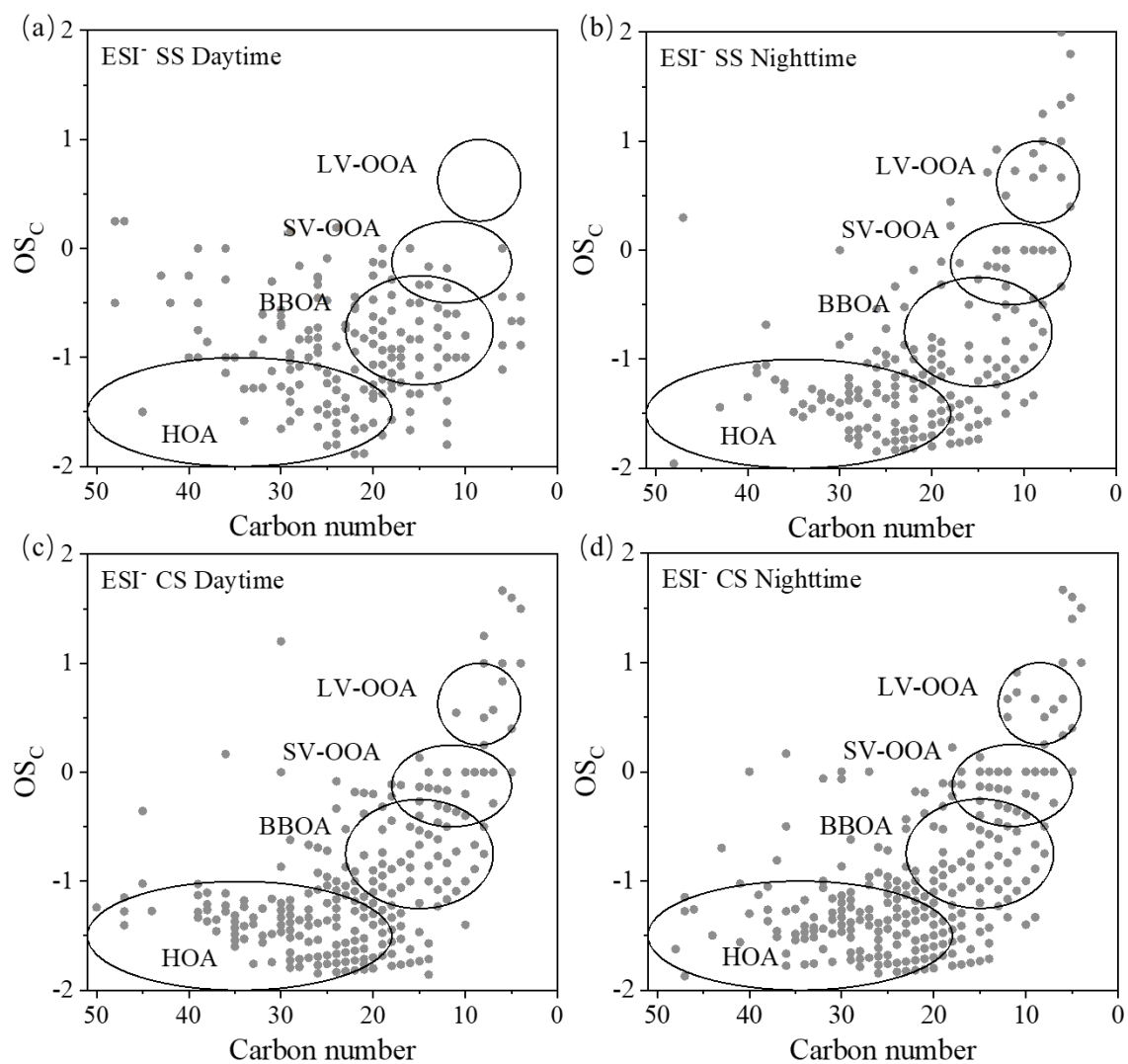
Figure S12. Scatter plots of the carbon oxidation state (OSc) versus carbon number for all CHO compounds in ESI⁻ mode during different periods. (a) SS daytime, (b) SS nighttime, (c) CS daytime, and (d) CS nighttime. Meanings of the circled areas are same as those described in Figure S11.
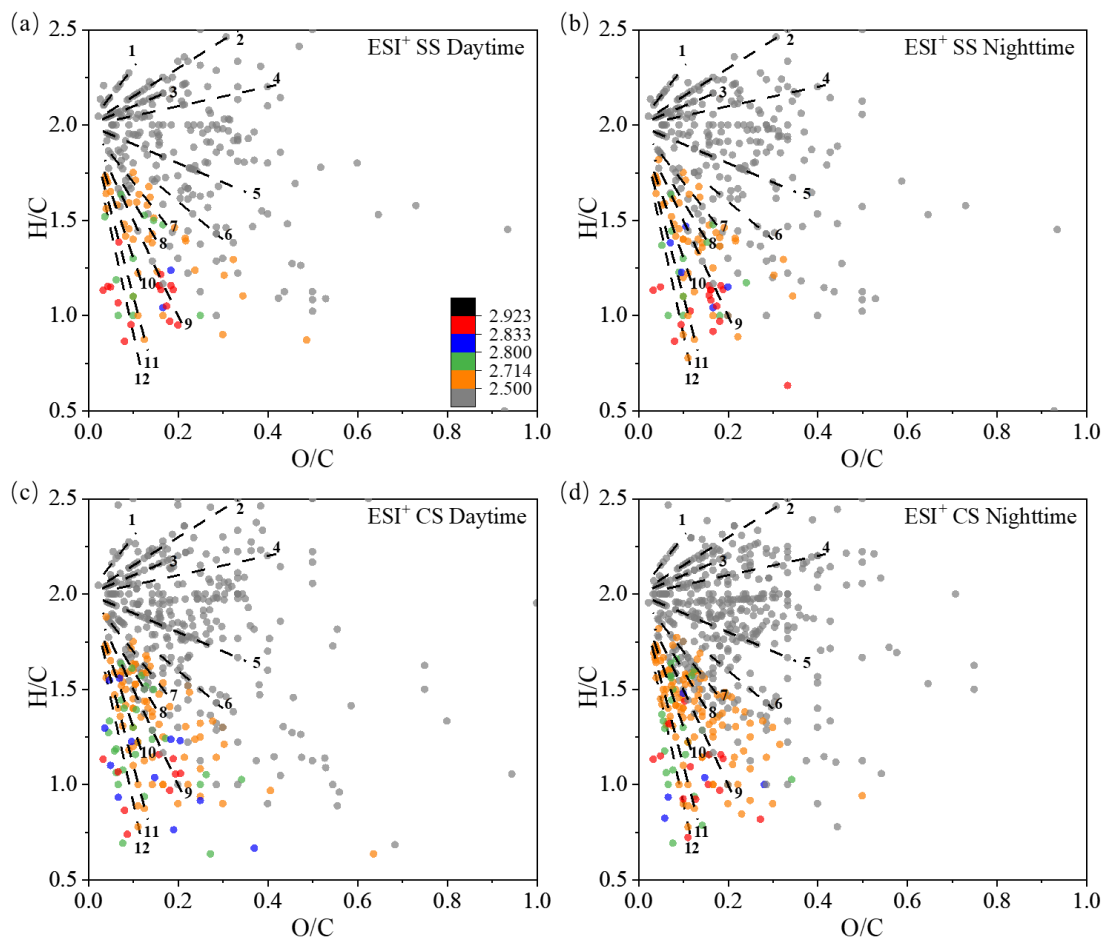
Figure S13. Van Krevelen diagram for CHON compounds detected in ESI$^+$ mode during different periods. (a) SS daytime, (b) SS nighttime, (c) CS daytime, and (d) CS nighttime. The markers with different colors represent aliphatic compounds ($Xc < 2.50$), aromatic benzene ring structures ($2.50 \leq Xc < 2.71$), naphthalene ring structures ($2.71 \leq Xc < 2.80$), anthracene ring structures ($2.80 \leq Xc < 2.83$), and pyrene ring structures ($2.83 \leq Xc < 2.92$), respectively (Mao et al., 2022); Different dash lines represent different series of compounds.
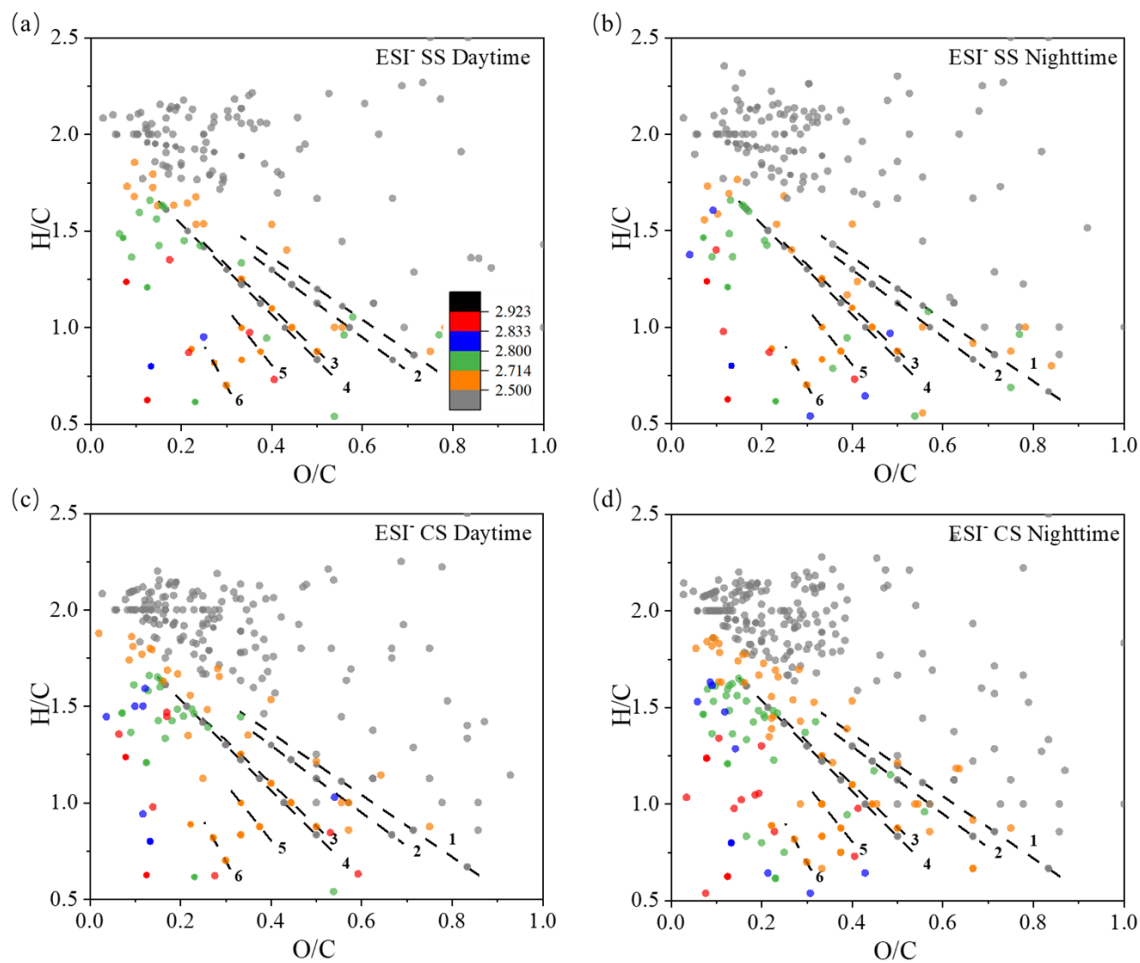
Figure S14. Van Krevelen diagram for CHON compounds detected in ESI⁻ mode during different periods. (a) SS daytime, (b) SS nighttime, (c) CS daytime, and (d) CS nighttime. Meanings of the clored values and dash lines are same as those described in Figure S13.
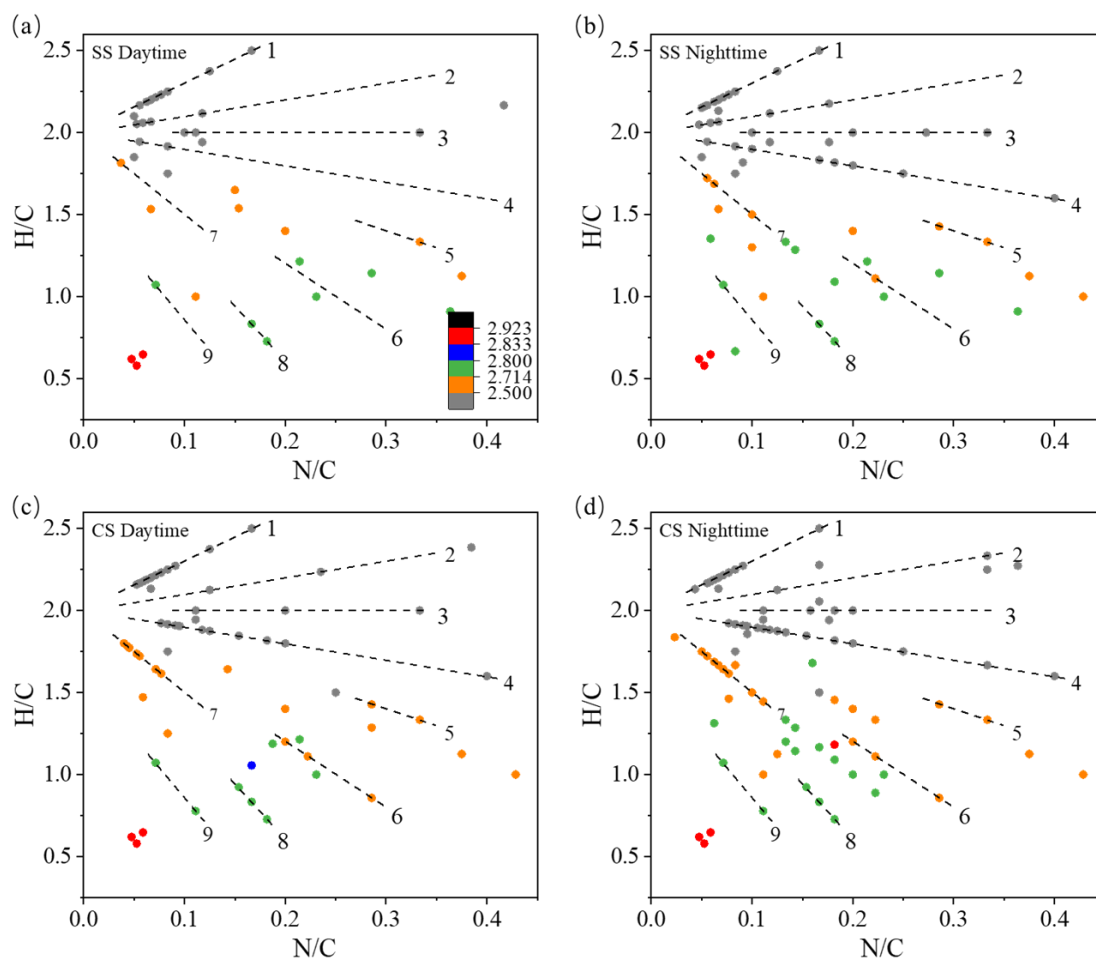
Figure S15. Van Krevelen diagram for CHN compounds detected in ESI$^+$ mode during different periods. (a) SS daytime, (b) SS nighttime, (c) CS daytime, and (d) CS nighttime. Meanings of the clored values and dash lines are same as those described in Figure S13.

## References

Al-Abadleh, H. A., Motaghedi, F., Mohammed, W., Rana, M. S., Malek, K. A., Rastogi, D., Asa-Awuku, A. A., and Guzman, M. I.: Reactivity of aminophenols in forming nitrogen-containing brown carbon from iron-catalyzed reactions, Commun. Chem., 5, 112, https://doi.org/10.1038/s42004-022-00732-1, 2022.

Aurell, J., Gullett, B. K., and Tabor, D.: Emissions from southeastern U.S. Grasslands and pine savannas: Comparison of aerial and ground field measurements with laboratory burns, Atmos. Environ., 111, 170-178, https://doi.org/10.1016/j.atmosenv.2015.03.001, 2015.

Chen, K. P., Raeofy, N., Lum, M., Mayorga, R., Woods, M., Bahreini, R., Zhang, H. F., and Lin, Y. H.: Solvent effects on chemical composition and optical properties of extracted secondary brown carbon constituents, Aerosol Sci. Technol., 56, 917-930, https://doi.org/10.1080/02786826.2022.2100734, 2022.

Huang, R. J., Yang, L., Shen, J. C., Yuan, W., Gong, Y. Q., Ni, H. Y., Duan, J., Yan, J., Huang, H. B., You, Q. H., and Li, Y. J.: Chromophoric fingerprinting of brown carbon from residential biomass burning, Environ. Sci. Technol. Lett., 9, 102-111, https://doi.org/10.1021/acs.estlett.1c00837, 2022.

Kourtchev, I., Godoi, R. H. M., Connors, S., Levine, J. G., Archibald, A. T., Godoi, A. F. L., Paralovo, S. L., Barbosa, C. G. G., Souza, R. A. F., Manzi, A. O., Seco, R., Sjostedt, S., Park, J. H., Guenther, A., Kim, S., Smith, J., Martin, S. T., and Kalberer, M.: Molecular composition of organic aerosols in central Amazonia: an ultra-high-resolution mass spectrometry study, Atmos. Chem. Phys., 16, 11899-11913, https://doi.org/10.5194/acp-16-11899-2016, 2016.

Kroll, J. H., Donahue, N. M., Jimenez, J. L., Kessler, S. H., Canagaratna, M. R., Wilson, K. R., Altieri, K. E., Mazzoleni, L. R., Wozniak, A. S., Bluhm, H., Mysak, E. R., Smith, J. D., Kolb, C. E., and Worsnop, D. R.: Carbon oxidation state as a metric for describing the chemistry of atmospheric organic aerosol, Nat. Chem., 3, 133-139, https://doi.org/10.1038/nchem.948, 2011.

Kuang, Y., Shang, J., and Chen, Q. C.: Effect of ozone aging on light absorption

and fluorescence of brown carbon in soot particles: The important role of polycyclic aromatic hydrocarbons, J. Hazard. Mater., 413, 125406, https://doi.org/10.1016/j.jhazmat.2021.125406, 2021.

Kuang, Y., Shang, J., Sheng, M. S., Shi, X. D., Zhu, J. L., and Qiu, X. H.: Molecular Composition of Beijing PM(2.5) Brown Carbon Revealed by an Untargeted Approach Based on Gas Chromatography and Time-of-Flight Mass Spectrometry, Environ. Sci. Technol., 57, 909-919, https://doi.org/10.1021/acs.est.2c05918, 2023.

Le Person, A., Lacoste, A., and Cornard, J.: Photo-degradation of trans-caffeic acid in aqueous solution and influence of complexation by metal ions, J. Photochem. Photobiol., A, 265, 10-19, https://doi.org/10.1016/j.jphotochem.2013.05.004, 2013.

Li, M., Wang, X. F., Lu, C. Y., Li, R., Zhang, J., Dong, S. W., Yang, L. X., Xue, L., Chen, J. M., and Wang, W. X.: Nitrated phenols and the phenolic precursors in the atmosphere in urban Jinan, China, Sci. Total Environ., 714, 136760, https://doi.org/10.1016/j.scitotenv.2020.136760, 2020.

Ma, Y. L. and Hays, M. D.: Thermal extraction – two-dimensional gas chromatography–mass spectrometry with heart-cutting for nitrogen heterocyclics in biomass burning aerosols, J. Chromatogr. A, 1200, 228-234, https://doi.org/10.1016/j.chroma.2008.05.078, 2008.

Mao, J. F., Cheng, Y., Bai, Z., Zhang, W., Zhang, L. Y., Chen, H., Wang, L. N., Li, L., and Chen, J. M.: Molecular characterization of nitrogen-containing organic compounds in the winter North China Plain, Sci Total Environ, 838, 156189, https://10.1016/j.scitotenv.2022.156189, 2022.

Negron-Encarnacion, I. and Arce, R.: Light-induced transformations of aza-aromatic pollutants adsorbed on models of atmospheric particulate matter: Acridine and 9(10-H) acridone, Atmos. Environ., 41, 6771-6783, https://doi.org/10.1016/j.atmosenv.2007.04.062, 2007.

Tong, H. J., Kourtchev, I., Pant, P., Keyte, I. J., O'Connor, I. P., Wenger, J. C., Pope, F. D., Harrison, R. M., and Kalberer, M.: Molecular composition of organic aerosols at urban background and road tunnel sites using ultra-high resolution mass spectrometry,

Faraday Discuss., 189, 51-68, https://doi.org/10.1039/C5FD00206K, 2016.

Yassine, M. M., Harir, M., Dabek-Zlotorzynska, E., and Schmitt-Kopplin, P.: Structural characterization of organic aerosol using Fourier transform ion cyclotron resonance mass spectrometry: Aromaticity equivalent approach, Rapid Commun. Mass Spectrom., 28, 2445-2454, https://doi.org/doi.org/10.1002/rcm.7038, 2014.

Zhang, S. Y.: Detection of scopolamine in nori fruit juice and its traditional chinese medicine compound health products by high performance liquid chromatography, World Latest Medicine Information, 18, 91-92, https://doi.org/10.19613/j.cnki.1671-3141.2018.82.066, 2018.